www.springer.com/41230
https://doi.org/10.1007/s41230-025-4199-6

On microstructure and room-/high-temperature properties of an Al_2O_3/Al-Cu-Mn composite

Jing-bin Liu, Jing-yi Hu, Meng-yu Li, Gui-liang Liu, *Tong Gao, and Xiang-fa Liu

Key Laboratory for Liquid-Solid Structural Evolution and Processing of Materials, Ministry of Education, Shandong University, Jinan 250061, China

Abstract: An Al_2O_3/Al-Cu-Mn composite was fabricated using a combination of ball milling and liquid-solid reaction, with a nominal composition of Al-4Cu-0.5Mn-2.8γ-Al_2O_3. The composite contains reinforcement particles, including nano-sized θ' and T($Al_{20}Cu_2Mn_3$) particles after T6 heat treatment, as well as in-situ synthesized nano-sized γ-Al_2O_3 particles. Tensile tests of the Al-4Cu-0.5Mn-2.8γ-Al_2O_3 composite and the Al-4Cu-0.5Mn base alloy after T6 treatment were carried out at room temperature and elevated temperatures (200 °C, 300 °C, and 400 °C). Compared with the base alloy, the yield strength of the Al-4Cu-0.5Mn-2.8γ-Al_2O_3 composite after T6 treatment increases significantly from 187 MPa to 263 MPa at room temperature. Simultaneously, at elevated temperatures, the yield strength is also enhanced, with a yield strength of 52 MPa at 400 °C for this composite. The in-situ fabricated γ-Al_2O_3 particles, mainly distributed along the grain boundaries, are supposed to play the main strengthening role, especially at high temperatures. This work acts as a reference for designing composites for high-temperature applications.

Keywords: Al matrix composite; mechanical strength; microstructure; Al_2O_3

CLC numbers: TG146.21 **Document code:** A **Article ID:** 1672-6421(2025)04-471-09

1 Introduction

Al-Cu-Mn-based alloys are widely used in aerospace and automotive industries due to their lightweight and high strength [1, 2]. In recent years, extensive research has focused on utilizing elements such as Zr, Sc, Er, and Gd to further improve the tensile strength of the alloys [3, 4]. However, the concept by increasing alloying element content to enhance the tensile properties of Al-Cu-Mn-based alloys is limited, as the alloys are highly susceptible to casting defects during solidification when the element content is high to some extent, e.g., porosity, hot tearing, and segregation, which can significantly degrade the mechanical properties of the alloys [5]. Except for traditional alloying theory, the development of aluminum matrix composites (AMCs) has attracted much attention due to their typically low density, high strength, and excellent high-temperature (HT) properties [6, 7]. The desired material is achieved by controlling the type, morphology characteristics, size, and distribution of the reinforcing particles in the matrix.

Currently, AMCs are mainly fabricated by either ex-situ or in-situ methods. The ex-situ methods, such as the casting method (e.g., melt-stirring [8] and squeeze casting [9]), are commonly used to prepare the AMCs. However, the problem of poor wettability at the interface between the Al matrix and reinforcing particles, results in a susceptibility of the interface to contamination [10, 11]. In contrast, in-situ methods exhibit obvious advantages in overcoming these drawbacks [12]. The in-situ methods are mainly based on the in-situ synthesis of ceramic particles and related intermetallic compounds as reinforcements through aluminum thermal substitution reaction between Al and precursors [13]. Reinforcements generated via in-situ methods are characterized by their non-pollution interfaces with the matrix and excellent high-temperature stability [14]. Thus, in-situ methods have received extensive attention and development in recent years, with self-propagating synthesis [15] and liquid-solid

*Tong Gao

Born in 1988, Ph. D., Professor. His research interests focus on heat-resistant and high-strength Al/Mg alloys, Al matrix composites, melt processing, and the design of special light alloy materials.

E-mail: tgao@sdu.edu.cn

Received: 2024-09-20; Revised: 2024-11-11; Accepted: 2024-12-16

reaction [16, 17] being commonly utilized techniques. For instance, Hu et al. [18] prepared a novel (8.5wt.% Al_3BC+14.5wt.% Al_2O_3)/Al composite by liquid-solid reaction method, exhibiting an ultimate tensile strength (UTS) of 188 MPa and an elongation (EL) of 4.4% at 350 °C. At present, ceramic reinforcement particles are widely studied in AMCs such as TiC [19], SiC [20], Al_2O_3 [21], AlN [22], etc. Among them, Al_2O_3 particles have received more attention due to their low density, high melting point, and high strength. Nano-Al_2O_3 particles generated by in-situ methods can be distributed along grain boundaries (GBs), effectively blocking GB sliding [23], e.g., an Al_2O_3/Al-Cu composite was fabricated in previous work, which exhibited a UTS of 420 MPa and an EL of 5.7% [24]. There are many metal oxides (MOs) commonly used for the preparation of Al_2O_3-reinforced AMCs, e.g., Fe_2O_3 [25], CuO [26], Ti_2O [27], and ZrO_2 [28]. Among amounts of Al-MO systems, CuO becomes one of the most applied precursors. For instance, Rong et al. [29] fabricated Al-5wt.% CuO, which can achieve UTS of 481 MPa, along with an EL of 16.8% at room temperature (RT). The reduced Cu atoms from CuO can be effectively dissolved into the Al matrix and subsequently precipitate as nano-sized θ' particles after aging treatment, which serve as reinforcements [30, 31].

In this study, based on our current research [24, 32], Al-5CuO-0.8MnO_2 (all components in this paper are wt.% unless otherwise noted) composite were fabricated via a combination of ball milling, liquid-solid reaction, and hot extrusion, aiming to design a composite with enhanced tensile properties. For comparison, an Al-4%Cu-0.5%Mn alloy was also prepared. The microstructure and mechanical properties of the composite and alloy were analyzed.

2 Experimental methods

2.1 Materials and composite fabrication

Raw materials used in this study included pure Al powder (99.9%, ~1 μm), copper oxide (CuO) powder (99.9%, ~50 nm), and manganese dioxide (MnO_2) powder (99.9%, ~50 nm). The weight ratio of Al, CuO, and MnO_2 powder was 94.2:5:0.8 and then ball milled using a planetary ball mill at 360 r·min^{-1} for 3 h. The ball-milled powder was put into a cylindrical rubber mold and then pressed through a cold isostatic press (LDJ200/500-380YS) at a pressure of 210 MPa to form a cylindrical blank. Then, the cylindrical blank was sintered in a vacuum sintering furnace (ZM-39-13) at 690 °C for 15 min. The sintered billet underwent hot extrusion at 460 °C with an extrusion ratio of 20:1. Through the in-situ chemical reactions between Al, CuO, and MnO_2, the final composite achieved was Al-4Cu-0.5Mn-2.8γ-Al_2O_3, namely Al-5CuO-0.8MnO_2 composite. For comparison, an Al-4%Cu-0.5%Mn alloy with the composition of Al-4Cu-0.5Mn was fabricated by hot extrusion an as-cast ingot using similar parameters [33]. Both bars were then subjected to T6 heat treatment, which involved solid solution treatment at 520 °C for 24 h followed by immediately quenched in water and an aging treatment at 185 °C for 48 h with subsequent air cooling.

2.2 Microstructure characterization

Phase characterization of Al-5CuO-0.8MnO_2 composite and Al-4Cu-0.5Mn alloy was carried out using X-ray diffraction (XRD, Rigaku D/max-rB, Tokyo, Japan) with Cu Kα radiation. The microstructure was analyzed using a field emission scanning electron microscope (FESEM, SU-70, Hitachi, Tokyo, Japan) equipped with an energy dispersive X-ray spectrometer (EDS). Grain size and Kernel average misorientation (KAM) were analyzed using a FESEM (FEI Verios 5 UC, FEI Company, Hillsboro, OR, USA) equipped with an EBSD detector (Symmetry S2, UK), and the data were processed using Channel 5 software. Transmission electron microscopy (TEM, FEI Talos F200X, 200 kV) with EDS capability was employed to observe the morphology and distribution of nano-precipitated particles. TEM samples were initially mechanically polished to a thickness of approximately 50 μm, then shaped into 3 mm circular discs using a perforating machine, and finally polished to a central perforation using an ion polishing system (Gatan 695, Pleasanton, CA, USA) for detailed observation.

2.3 Tensile test

The T6 heat-treated Al-5CuO-0.8MnO_2 composite and Al-4Cu-0.5Mn alloy test bars were machined into "dog-bone" shaped specimens for RT and HTs (200 °C, 300 °C, and 400 °C) tensile testing. The RT and HT tensile tests were carried out on a universal tensile testing machine (CMT700) with a loading rate of 2 mm·min^{-1}. To ensure the accuracy of the tests, three specimens were tested at each temperature and the average value was taken. The required specimen sizes of RT and HT tensile tests are shown in Fig. 1.

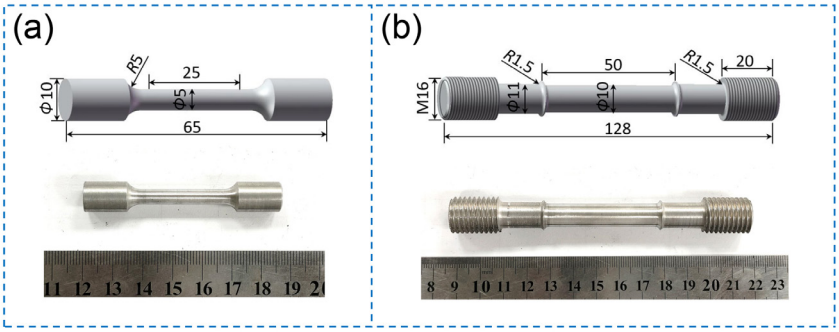

Fig. 1: Dimensions of tensile test specimens at different temperatures: (a) RT; (b) HT (unit: mm)

3 Results and discussion

Figure 2 shows the microstructure of the Al-5CuO-0.8MnO_2 composite and the Al-4Cu-0.5Mn alloy along the longitudinal section. The Al_2Cu phases determined by EDS analysis [(Fig. 2(b)] in the as-extruded composite are distributed along the extrusion direction [Fig. 2(a)]. It can also be seen that the quantity of Al_2Cu phases is significantly decreased in Fig. 2(c), indicating that the Al_2Cu phases have been dissolved into the Al matrix during the solution treatment. Figure 2(d) shows a magnified area of the marked Region B in Fig. 2(c), revealing that Al and CuO have synthesized a large number of Al_2O_3 particles by an in-situ reaction. Figure 2(e) shows the microstructure of the aging-treated composite. Many fine rod-like white particles (indicated by yellow arrows) and larger gray particles (indicated by a blue arrow) are found in the yellow magnified area, and further analysis will be conducted using TEM. Figures 2(f–g) exhibit the microstructure of the as-extruded and solid solution-treated Al-4Cu-0.5Mn base alloy. The distribution of the Al_2Cu phase confirmed by mapping [Fig. 2(h)] is also oriented along the extrusion direction in Fig. 2(f). In addition, the Al_2Cu phase during the solution treatment [Fig. 2(g)] is also largely incorporated into the Al matrix compared to the as-extruded base alloy [Fig. 2(f)].

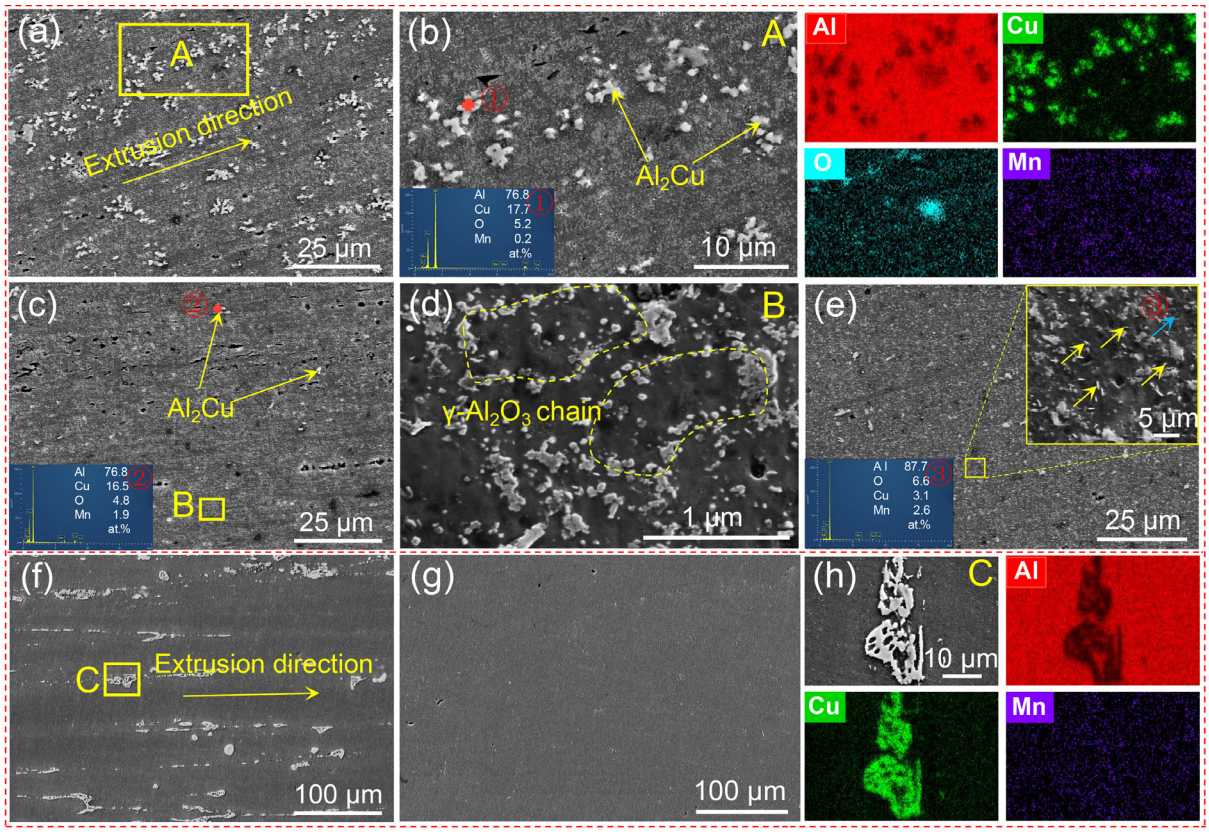

Fig. 2: SEM microstructures of Al-5CuO-0.8MnO_2 composite (a–e) and Al-4Cu-0.5Mn alloy (f–h) in longitudinal section: (a) microstructure of as-extruded composite; (b) magnified area of marked Region A in (a) and its mapping (the inset shows point analysis at Point 1); (c) microstructure of solution-treated composite (the inset shows the point analysis at Point 2); (d) the magnified area of marked Region B in (c); (e) microstructure of aging-treated composite (the inset shows point analysis at Point 3); (f, g) microstructure of as-extruded and solution-treated base alloy, respectively; (h) mapping of magnified area of marked Region C in (f)

Figure 3 exhibits the XRD patterns of the Al-5CuO-0.8MnO_2 composite with the as-extruded, solid solution-treated, and aging-treated methods along the longitudinal section. Based on the standard XRD database [34], the Al_2Cu peak (PDF#89-1981) and γ-Al_2O_3 peak (PDF#23-1009) are successfully detected, which is consistent with our previous work [32]. It is also found that the diffraction peaks of Al_2Cu disappear in the solution treatment and reappear in the aging treatment. This indicates the dissolution of the Al_2Cu phases and reprecipitation of the nano-sized θ'(Al_2Cu) phases, respectively, aligning with the observations presented in Fig. 2.

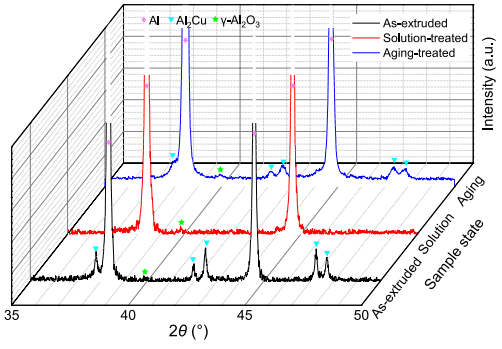

Fig. 3: XRD patterns of Al-5CuO-0.8MnO_2 composite after extrusion, solution, and aging

Typical EBSD results of the Al-5CuO-0.8MnO_2 composite and the Al-4Cu-0.5Mn alloy after T6 treatment are shown in Fig. 4. As can be found in Figs. 4(a) and (b), the equiaxed grains and elongated grains together constitute the microstructure of the Al-5CuO-0.8MnO_2 composite, while the Al-4Cu-0.5Mn alloy is mainly composed of elongated grains. The statistical grain size of the Al matrix in the Al-5CuO-0.8MnO_2 composite is 0.71 μm, which is much smaller than that of 82.95 μm in the Al-4Cu-0.5Mn alloy, as shown in Figs. 4(c) and (d). Figures 4(e) and (f) demonstrate the KAM map of the Al-5CuO-0.8MnO_2 composite and the Al-4Cu-0.5Mn alloy after T6 treatment, respectively. The Al-5CuO-0.8MnO_2 composite has a larger KAM value than the Al-4Cu-0.5Mn alloy [seen in Fig. 4(g)], indicating a higher dislocation density in the composite [35]. Based on Figs. 4(e) and (f), the density of geometrically necessary dislocations (GNDs) is calculated to be 6.2×10^{13} m^{-2} for the Al-5CuO-0.8MnO_2 composite and 5.4×10^{11} m^{-2} for the Al-4Cu-0.5Mn alloy, respectively. This phenomenon, combined with the fine matrix grain size, may be due to the formation of nano-sized Al_2O_3 particles, which can cause an increase in residual stresses or micro-zone deformation inhomogeneity in the composite. Figure 4(h) displays the statistics of the Schmid factor for the Al-5CuO-0.8MnO_2 composite and the Al-4Cu-0.5Mn alloy after T6 treatment, i.e., 0.43 and 0.47, respectively. This suggests that the generation of nano-sized Al_2O_3 particles does not affect the deformability of the composite [36].

Figure 5 presents the typical microstructure of the Al-5CuO-0.8MnO_2 composite after T6 treatment. The presence of needle-like, plate-like, and block-like particles is observed in Fig. 5(a). The EDS mapping in Figs. 5(a1–a3) as well as the inserted selected area electron diffraction (SAED) pattern confirms that these phases are Al_2Cu. Figure 5(b) shows a magnified image of the marked Region A in Fig. 5(a). Both the needle and plate phases are identified as θ'(Al_2Cu) by high-resolution analysis of the marked Regions B and C, respectively [Figs. 5(c) and (d)]. Two kinds of morphologies occur since they are viewed from different directions on the flake-like shape. Meanwhile, the inserted D and E fast fourier transform (FFT) images further confirm this result. The diameter of θ' phase was counted in Fig. 5(e). The average length of the θ' phase in the Al-5CuO-0.8MnO_2 composite reaches 103 nm. Figures 5(f) and (g) exhibit the high-angle annular dark field (HAADF) and bright field (BF) images of the Al-4Cu-0.5Mn alloy after T6 treatment, respectively, and the corresponding SAED plots are shown in Fig. 5(h). It can be found that there are both needle-like and plate-like θ' particles. The average diameter of θ' phases in Al-4Cu-0.5Mn alloy is 131 nm. Meanwhile, it can be clearly observed that the particle density of θ' in Al-5CuO-0.8MnO_2 composite [Fig. 5(a)] is much less than that in Al-4Cu-0.5Mn alloy [Fig. 5(f)].

Figures 6(a) and (b) illustrate the HAADF images of both T6-treated Al-5CuO-0.8MnO_2 composite and Al-4Cu-0.5Mn alloy as well as their corresponding elemental distributions [Figs. 6(a1) and (b1)]. It can be clearly seen that Mn-rich phases with block-like and rod-like morphologies are present in both materials. Quantitative analysis indicates that the density of Mn-rich phases in the Al-5CuO-0.8MnO_2 composite is less than that in the Al-4Cu-0.5Mn alloy. It has been reported that another reinforcing phase, the T($Al_{20}Cu_2Mn_3$) phase, exists in the Al-Cu-Mn-based alloys [1]. The block-like T phase [Fig. 2(e)] is probably obtained from the decomposition of Phase I ($Al_{13}Cu_4Mn_3$) during the solid solution treatment, while the rod-like phase forms by direct precipitation during aging treatment [1, 37]. This corresponds to the phases identified by the blue and yellow arrows in Fig. 2(e). Figure 6(c) shows a TEM image of a single Al grain and the EDS mappings [Fig. 6(c1)]. It is observed that γ-Al_2O_3 is mainly distributed along the GBs of Al grain, with only a few particles presented within the grain itself.

Engineering stress-strain curves for the Al-5CuO-0.8MnO_2 composite and Al-4Cu-0.5Mn alloy after T6 treatment were tested at RT, 200 °C, 300 °C, and 400 °C, as depicted in Fig. 7. The corresponding yield strength (YS), UTS, and EL

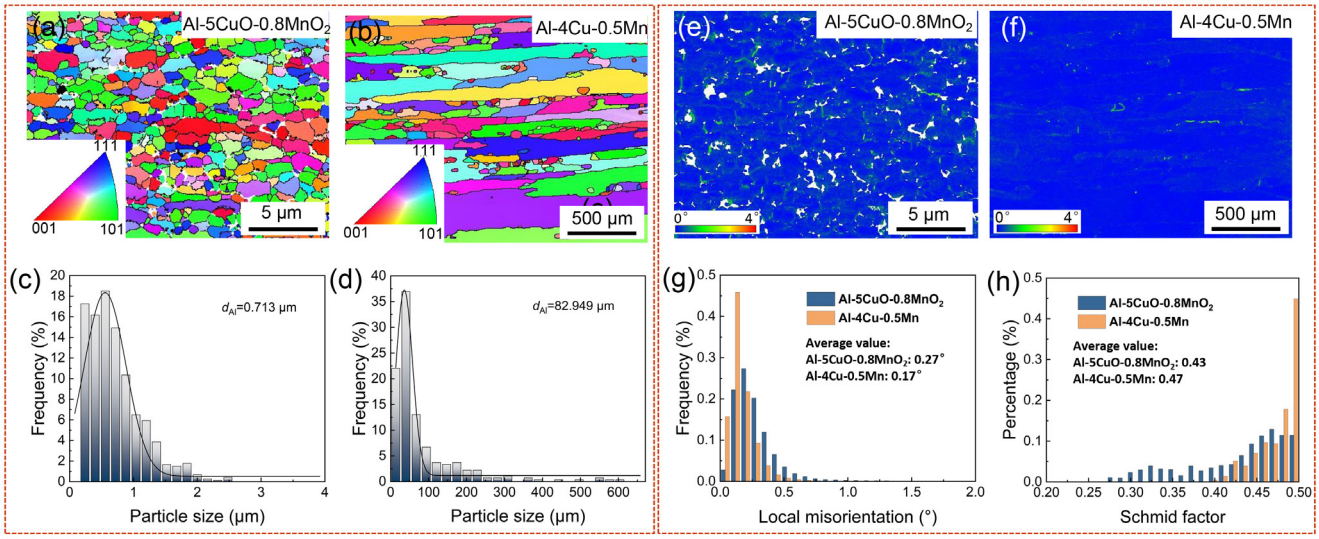

Fig. 4: EBSD characterization of Al-5CuO-0.8MnO_2 composite and Al-4Cu-0.5Mn alloy after T6 treatment: (a, b) orientation map; (c, d) grain size; (e, f) KAM map; (g) KAM distribution; (h) Schmid factor distribution

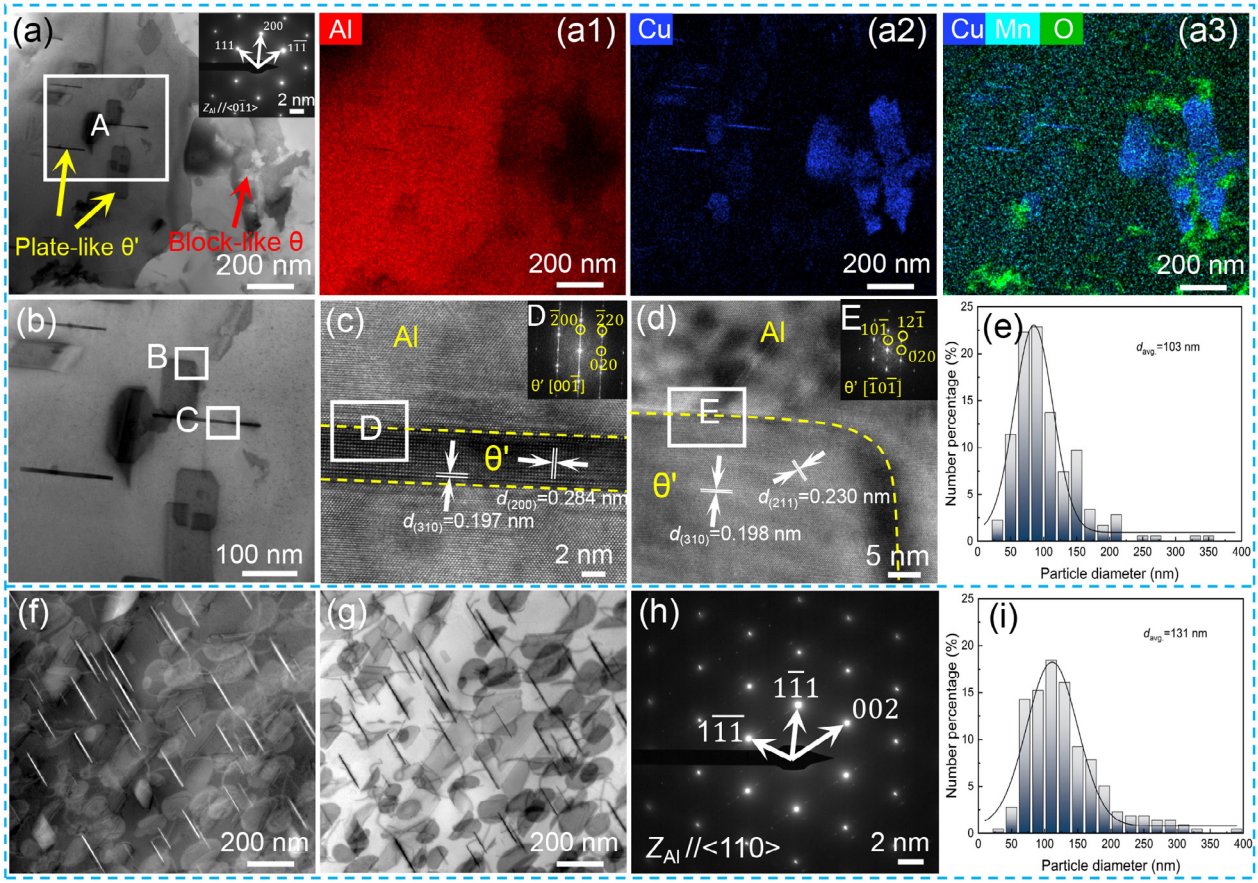

Fig. 5: TEM microstructures and diameter size distribution of Al-5CuO-0.8MnO_2 composite (a–e) and Al-4Cu-0.5Mn alloy (f–i) after T6 treatment: (a) BF image and SAED pattern; (a1–a3) EDS mapping of Al-5CuO-0.8MnO_2 composite; (b) magnified area of marked Region A in (a); (c) and (d) are the high-resolution of magnified area of marked Region B and C in (c) (inserted FFT D and FFT E recorded the marked Regions D and E, respectively); (e) diameter size distribution of θ' particles in Al-5CuO-0.8MnO_2 composite; (f and g) HAADF and BF images of Al-4Cu-0.5Mn alloy; (h) SAED pattern of (f); (i) diameter size distribution of θ' particles in Al-4Cu-0.5Mn alloy

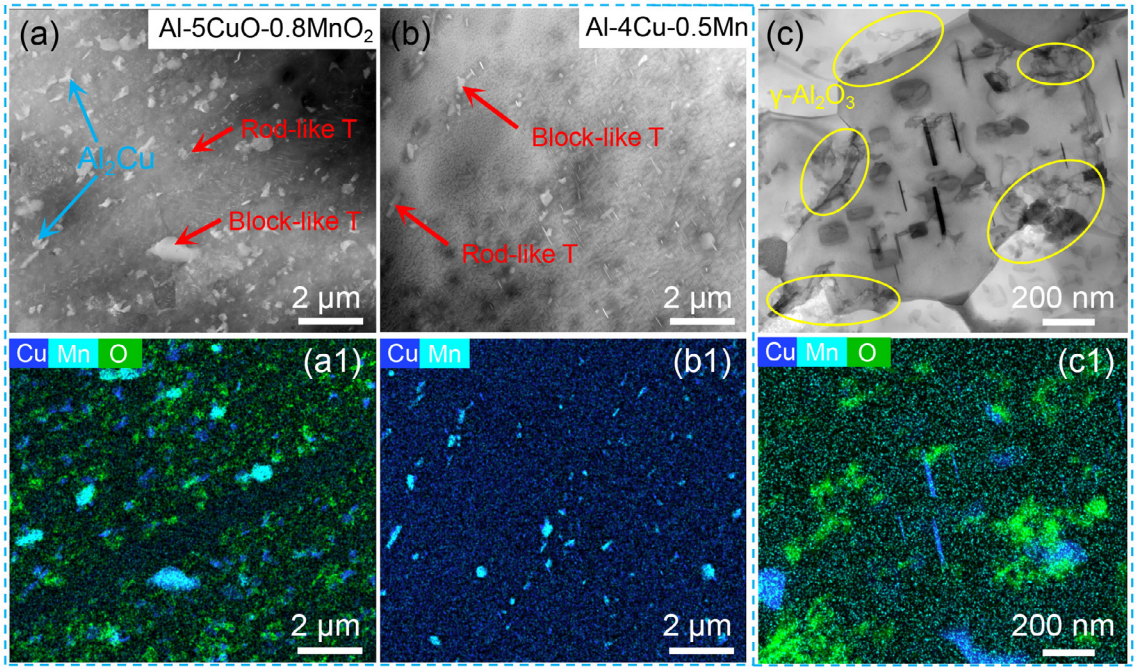

Fig. 6: TEM microstructure of Al-5CuO-0.8MnO_2 composite and Al-4Cu-0.5Mn alloy after T6 treatment: HAADF images (a, b) and EDS mapping (a1, b1) of Al-5CuO-0.8MnO_2 composite and Al-4Cu-0.5Mn alloy, respectively; HAADF image (c) and EDS mapping (c1) of a single grain in Al-5CuO-0.8MnO_2 composite

results are exhibited in Table 1. It is found that the YS and UTS values of both the Al-5CuO-0.8MnO_2 composite and Al-4Cu-0.5Mn alloy after T6 treatment decrease with increasing testing temperature, indicating that the Al matrix undergoes high-temperature softening. At RT, the YS of the Al-5CuO-0.8MnO_2 composite after T6 treatment is 263 MPa, which is a 41% increase compared to 187 MPa for the Al-4Cu-0.5Mn alloy after T6 treatment. Moreover, the YS of T6-treated Al-5CuO-0.8MnO_2 composite tested at 200 °C, 300 °C, and 400 °C are 171 MPa, 98 MPa, and 52 MPa, respectively, which are 14%, 8%, and 53% higher than that of T6-treated Al-4Cu-0.5Mn alloy. This indicates that the Al-5CuO-0.8MnO_2 composite treated by T6 exhibits superior high-temperature strength than that of the Al-4Cu-0.5Mn alloy treated by T6, probably related to the presence of γ-Al_2O_3 particles.

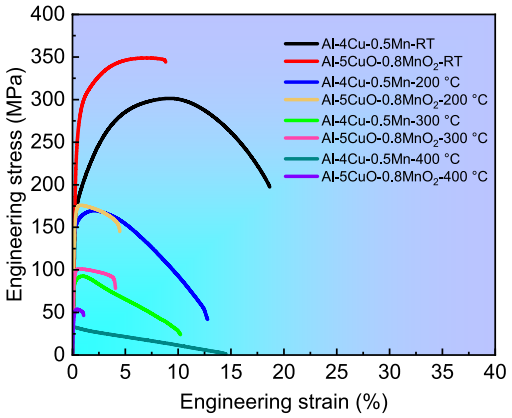

Fig. 7: Typical tensile engineering stress-strain curves of Al-5CuO-0.8MnO_2 composite and Al-4Cu-0.5Mn alloy after T6 treatment tested at RT, 200 °C, 300 °C, and 400 °C

Table 1: Mechanical properties of Al-5CuO-0.8MnO_2 composite and Al-4Cu-0.5Mn alloy after T6 treatment

Tensile test temperatures	Materials	YS (MPa)	UTS (MPa)	EL (%)
RT	Al-4Cu-0.5Mn	187±18	305±15	18.3±0.4
	Al-5CuO-0.8MnO_2	263±3	347±7	9.0±0.6
200 °C	Al-4Cu-0.5Mn	150±19	169±15	12.8±1.7
	Al-5CuO-0.8MnO_2	171±1	176±1	5.1±0.6
300 °C	Al-4Cu-0.5Mn	91±3	96±3	9.9±0.3
	Al-5CuO-0.8MnO_2	98±1	100±1	4.1± 0.1
400 °C	Al-4Cu-0.5Mn	34±1	34±1	14.9±0.4
	Al-5CuO-0.8MnO_2	52±2	53±2	1.1±0.1

The fracture microstructures of the Al-5CuO-0.8MnO_2 composite and the Al-4Cu-0.5Mn alloy after T6 treatment through tensile testing at RT, 200 °C, 300 °C, and 400 °C are shown in Fig. 8. Tearing ridges and various sizes of dimples are observed on the Al-4Cu-0.5Mn alloy fracture surfaces in Figs. 8(a–d), indicating typical ductile fracture characteristics. The presence of large and deep dimples at room-temperature and high-temperature suggests that this alloy has good plasticity. In the Al-5CuO-0.8MnO_2 composite [Figs. 8(e) and (f)], similar ductile fracture features are observed, with dimples of different sizes. However, compared to the Al-4Cu-0.5Mn alloy, these dimples are smaller and shallower in size, suggesting lower deformability for the Al-5CuO-0.8MnO_2 composite [38]. In addition, the dimple features are hardly visible in the fracture surface at 300 °C and 400 °C, as shown in Figs. 8(g) and (h), where intergranular fracture characteristics predominate. It has been reported that the dynamic recovery at GBs may lead to localized deformation, potentially initiating the generation of voids and cracks [39, 40]. As displayed in Figs. 8(g), relative sliding (indicated by yellow arrows) is found between neighboring grains on the fracture surfaces, indicating the occurrence of dynamic recovery at GBs. As a result, voids (red arrows) generate, which in turn leads to the fracture of the composite.

To further clarify the changes in strength and ductility of the T6-treated Al-5CuO-0.8MnO_2 composite tensile tested at room-temperature and high-temperature, the strengthening mechanism and tensile fracture morphologies of the Al-5CuO-0.8MnO_2 composite (Fig. 8) were analyzed. Despite the lower quantitative densities of θ' and T($Al_{20}Cu_2Mn_3$) reinforcements in the Al-5CuO-0.8MnO_2 composite compared to the Al-4Cu-0.5Mn alloy, as can be easily found in Figs. 5(b) and (f), the YS of the Al-5CuO-0.8MnO_2 composite still surpasses that of the Al-4Cu-0.5Mn alloy at room temperature. This enhancement is attributed to grain refinement strengthening and load-transfer strengthening due to the presence of nano-sized Al_2O_3 particles. The Hall-Petch relationship indicates that finer grains have higher YS [41]. After T6 treatment, the average grain size of the Al-5CuO-0.8MnO_2 composite is much smaller compared to that of the Al-4Cu-0.5Mn alloy (Fig. 4), resulting in the increased YS of the Al-5CuO-0.8MnO_2 composite. In addition, the in-situ synthesized nano-sized Al_2O_3

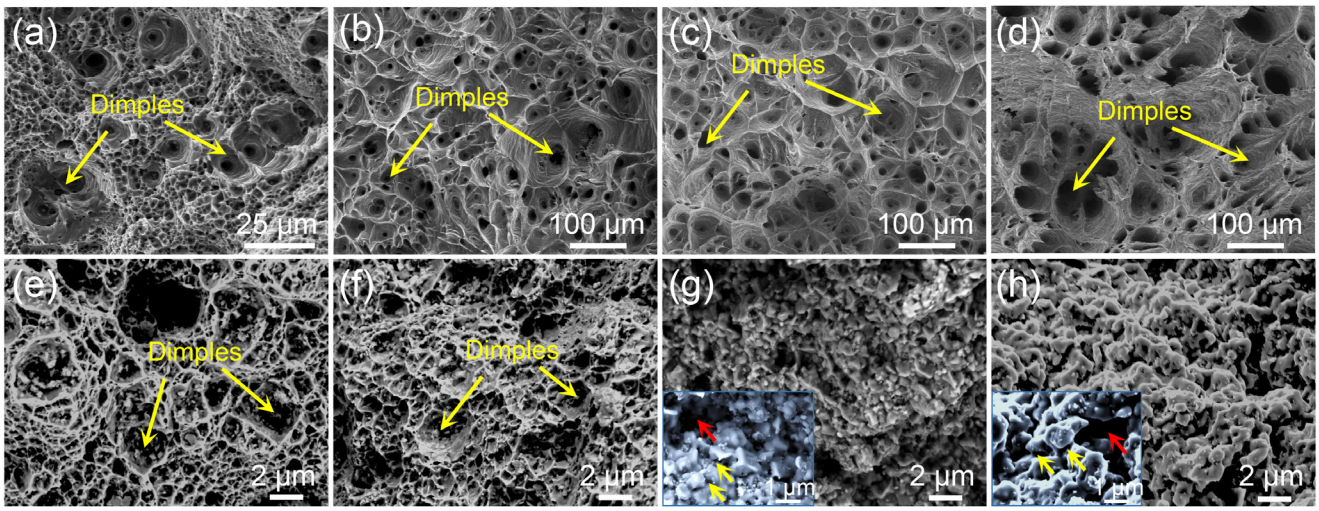

Fig. 8: Tensile fracture morphologies of Al-4Cu-0.5Mn alloy (a–d) and Al-5CuO-0.8MnO_2 composite (e–h) after T6 treatment: (a, e) RT; (b, f) 200 °C; (c, g) 300 °C; (d, h) 400 °C

particles provide additional strengthening effects. In general, their strengthening effects are usually realized in two ways: direct strengthening via load transfer and indirect secondary strengthening resulting from dislocation accumulation, which includes the Orowan strengthening mechanism and the strengthening due to GNDs [42-44]. For instance, the detected GNDs density of the Al-5CuO-0.8MnO_2 composite is far more larger than that of the Al-4Cu-0.5Mn alloy, indicating the existence of the abovementioned strengthening mechanism. Therefore, the combined effects of multiple strengthening mechanisms result in a favorable YS of the Al-5CuO-0.8MnO_2 composite at room temperature.

The θ' phase and T($Al_{20}Cu_2Mn_3$) phase can play a certain role in strengthening at lower temperatures but have limited effectiveness at higher temperatures, such as 300 °C and 400 °C, as discussed in this study. In comparison, the in-situ generated nano-sized Al_2O_3 particles maintain relatively good stability at high temperatures. Therefore, it is inferred that γ-Al_2O_3 particles play a major role in the strengthening of the Al-5CuO-0.8MnO_2 composite at high temperatures. Sliding of GBs and rotation of crystals at high temperatures lead to the release of dislocation accumulation at the GBs, thereby weakening their reinforcement capacity and softening the Al matrix [45]. However, the pinning effect of fine particles or nanoparticles can effectively prevent GB movement, thus improving the high temperature performance of the composites [39, 45, 46]. As illustrated in Fig. 6(c), the γ-Al_2O_3 particles are agglomerated along the GBs, exerting a pinning effect that contributes to improved high temperature tensile strength of the Al-5CuO-0.8MnO_2 composite.

Compared Fig. 8(f) with Fig. 8(e), it can be found that the number and size of dimples on the fracture surface of the Al-5CuO-0.8MnO_2 composite decrease to some extent when the testing temperature increases to 200 °C, resulting in lower deformability of the composite [38]. In addition, the dislocation density decreases at high temperatures due to the onset of dynamic recovery, leading to a reduction in the work-hardening effect [38]. Meanwhile, due to the occurrence of dynamic recovery, the dislocations interact with the Al_2O_3 particles at the GBs, leading to localized plastic deformation and the formation of cavities [40]. This interaction ultimately results in the development of intergranular fracture [Figs. 8(g) and (h)]. Collectively, the combined effect contributes to the decrease in the elongation of the Al-5CuO-0.8MnO_2 composite with increasing temperatures (Fig. 7).

4 Conclusions

In this work, the Al-5CuO-0.8MnO_2 composite was fabricated with a nominal composition of Al-4Cu-0.5Mn-2.8γ-Al_2O_3. The effects of intermetallic compounds and γ-Al_2O_3 particles on microstructure evolution, mechanical properties, and strengthening mechanisms at RT, 200 °C, 300 °C, and 400 °C were systematically investigated. An Al-4Cu-0.5Mn alloy was fabricated for comparison. The key results are summarized below:

(1) With a combination of sintering, hot extrusion, and T6 heat treatment, the achieved Al-5CuO-0.8MnO_2 composite contains θ', T($Al_{20}Cu_2Mn_3$) phases, and γ-Al_2O_3 particles. The γ-Al_2O_3 particles are mainly distributed along the GBs, resulting in a significantly finer matrix grain size in the T6 treated Al-5CuO-0.8MnO_2 composite compared to the T6 treated Al-4Cu-0.5Mn alloy.

(2) Compared with the T6-treated Al-4Cu-0.5Mn base alloy, the YS of the T6 treated Al-5CuO-0.8MnO_2 composite is enhanced from 187 MPa to 263 MPa at room temperatures, 150 MPa to 171 MPa at 200 °C, 91 MPa to 98 MPa at 300 °C, and 34 MPa to 52 MPa at 400 °C, respectively. The improvement is attributed to the positive strengthening effects of the in-situ γ-Al_2O_3 nanoparticles.

(3) By promoting chemical reactions between the Al matrix and metal oxides, Al_2O_3-reinforced AMCs may overcome the weakness of traditional Al alloys prepared using alloying methods, particularly in high temperature applications.

Acknowledgments

This research was financially supported by the National Natural Science Foundation of China (No. 52471040), and the Natural Science Foundation of Shandong Province (No. ZR2022ME005).

Conflict of interest

The authors declare that they have no competing financial interests or personal relationships that could have appeared to influence the work in this paper.

References

[1] Dar S M, Liao H C, Xu A Q. Effect of Cu and Mn content on solidification microstructure, T-phase formation and mechanical property of Al-Cu-Mn alloys. Journal of Alloys and Compounds, 2019, 774: 758–767.
[2] Zhang F, Guo T B, Li Q, et al. Effects of minor Y, Zr and Er addition on microstructure and properties of Al-5Cu-0.4Mn alloy. China Foundry, 2017, 14(6): 461–468.
[3] Lamb J, Rouxel B, Langan T, et al. Novel Al-Cu-Mn-Zr-Sc compositions exhibiting increased mechanical performance after a high-temperature thermal exposure. Journal of Materials Engineering and Performance, 2020, 29: 5672–5684.
[4] Ma C X, Rong L, Chen J S, et al. Effect of Er and Zr on hot crack resistance and mechanical properties of Al-Cu-Mn-Cd alloy. International Journal of Metalcasting, 2025, 19: 1388–1402.
[5] Li B, Shen Y F, Hu W Y, et al. Casting defects induced fatigue damage in aircraft frames of ZL205A aluminum alloy – A failure analysis. Materials & Design, 2011, 32: 2570–2582.
[6] Liu T S, Qiu F, Yang H Y, et al. Exploring the potential of FSW-ed Al-Zn-Mg-Cu-based composite reinforced by trace in-situ nanoparticles in manufacturing workpiece with customizable size and high mechanical performances. Composites, Part B: Engineering, 2023, 250: 110425.
[7] Yang H, Topping T D, Wehage K, et al. Tensile behavior and strengthening mechanisms in a submicron B_4C-reinforced Al trimodal composite. Materials Science and Engineering: A, 2014, 616: 35–43.
[8] Doel T J A, Bowen P. Tensile properties of particulate-reinforced metal matrix composites. Composites, Part A: Applied Science and Manufacturing, 1996, 27(8): 655–665.
[9] Seo Y H, Kang C G. Effects of hot extrusion through a curved die on the mechanical properties of SiC_p/Al composites fabricated by melt-stirring. Composites Science and Technology, 1999, 59(5): 643–654.
[10] Tham L M, Gupta M, Cheng L. Effect of limited matrix-reinforcement interfacial reaction on enhancing the mechanical properties of aluminium-silicon carbide composites. Acta Materialia, 2001, 49(16): 3243–3253.
[11] Daniel B S S, Murthy V S R, Murty G S. Metal-ceramic composites via in-situ methods. Journal of Materials Processing Technology, 1997, 68(2): 132–155.
[12] Gao T, Bian Y H, Li Z Q, et al. Synthesis of a ($ZrAl_3$+AlN)/Al composite and the influence of particles content and element Cu on the microstructure and mechanical properties. Journal of Alloys and Compounds, 2019, 791: 730–738.
[13] Zhao G, Shi Z M, Ta N, et al. Effect of the heating rate on the microstructure of in situ Al_2O_3 particle-reinforced Al matrix composites prepared via displacement reactions in an Al/CuO system. Materials & Design, 2015, 66: 492–497.
[14] Yang B, Sun M, Gan G S, et al. In situ Al_2O_3 particle-reinforced Al and Cu matrix composites synthesized by displacement reactions. Journal of Alloys and Compounds, 2010, 494(1–2): 261–265.
[15] Zhang M X, Huo Y Q, Ma L, et al. In situ TiC ceramic particles locally reinforced Al-Si matrix composites prepared by SHS-casting method from the Al-Si-Ti-C system. International Journal of Applied Ceramic Technology, 2014, 11(4): 723–731.
[16] Bian Y H, Gao T, Li Z Q, et al. In-situ synthesis of an Al composite reinforced with multi-scale $Al_{12}Mo$, (Al, Zr, Si) and Al_2O_3 particles through a multi-stage reaction. Materials Science and Engineering: A, 2019, 762: 138069.
[17] Zhao Y F, Qian Z, Ma X, et al. Unveiling the semicoherent interface with definite orientation relationships between reinforcements and matrix in novel Al_3BC/Al composites. ACS Applied Materials & Interfaces, 2016, 8(41): 28194–28201.
[18] Hu J Y, Gao T, Li M Y, et al. Synthesis of an (Al_3BC+Al_2O_3)/Al composite with high stiffness and attractive high-temperature tensile properties. Materials Research Letters, 2024, 12: 355–362.
[19] Wang W l, Shi K, Zhao J, et al. Corrosion and wear properties of in situ (TiB+TiC)/TA15 composites with a high volume percentage of reinforcement. China Foundry, 2023, 20(5): 423–431.
[20] Zhang Z M, Fan G L, Tan Z Q, et al. Towards the strength-ductility synergy of Al_2O_3/Al composite through the design of roughened interface. Composites, Part B: Engineering, 2021, 224: 109251.
[21] Mazahery A, Ostadshabani M. Investigation on mechanical properties of nano-Al_2O_3-reinforced aluminum matrix composites. Journal of Composite Materials, 2011, 45(24): 2579–2586.
[22] Xie K W, Nie J F, Liu C, et al. A novel Al-Cu composite with ultra-high strength at 350 °C via dual-phase particle reinforced submicron-structure. Advanced Science, 2023, 10(25): 2207208.
[23] Liu Y, Zan Y N, Wang D, et al. Design of a thermally stable heat-resistant (Al_2O_3+Al_3Ti)/Al composite with excellent high-temperature mechanical properties: Multimechanism synergistic strengthening strategy. Nano Letters, 2024, 24(33): 10244–10250.
[24] Gao T, Liu L Y, Song J P, et al. Synthesis and characterization of an in-situ Al_2O_3/Al-Cu composite with a heterogeneous structure. Journal of Alloys and Compounds, 2021, 868: 159283.
[25] Azimi-Roeen G, Kashani-Bozorg S F, Nosko M, et al. Reactive mechanism and mechanical properties of in-situ hybrid nano-composites fabricated from an Al-Fe_2O_3 system by friction stir processing. Materials Characterization, 2017, 127: 279–287.
[26] Dikici B, Gavgali M. The effect of sintering time on synthesis of in situ submicron α-Al_2O_3 particles by the exothermic reactions of CuO particles in molten pure Al. Journal of Alloys and Compounds, 2013, 551: 101–107.
[27] Zhang Q, Xiao B L, Wang W G, et al. Reactive mechanism and mechanical properties of in situ composites fabricated from an Al-TiO_2 system by friction stir processing. Acta Materialia, 2012, 60(20): 7090–7103.
[28] Zhu H G, Min J, Li J L, et al. In situ fabrication of (α-Al_2O_3+Al_3Zr)/Al composites in an Al-ZrO_2 system. Composites Science and Technology, 2010, 70(15): 2183–2189.
[29] Rong X D, Zhao D D, He C N, et al. Revealing the strengthening and toughening mechanisms of Al-CuO composite fabricated via in-situ solid-state reaction. Acta Materialia, 2021, 204: 116524.

[30] Roy S, Allard L F, Rodriguez A, et al. Comparative evaluation of cast aluminum alloys for automotive cylinder heads: Part II–Mechanical and thermal properties. Metallurgical and Materials Transactions: A, 2017, 48: 2543–2562.
[31] Shin D, Shyam A, Lee S, et al. Solute segregation at the Al/θ′-Al_2Cu interface in Al-Cu alloys. Acta Materialia, 2017, 141: 327–340.
[32] Li M Y, Li C X, Hu J Y, et al. Modify the interface between ex-situ γ-Al_2O_3 and Al matrix via in-situ coating in an Al matrix composite. Composites Communications, 2024, 47: 101860.
[33] Liu J B, Hu J Y, Li M Y, et al. Influence of Zr microalloying on the microstructure and room-/high-temperature mechanical properties of an Al-Cu-Mn-Fe alloy. Materials, 2024, 17(9): 2022.
[34] Swanson H E, Tatge E, Fuyat R K. Standard X-ray diffraction powder patterns. Physics Today, 1954, 7(8): 22.
[35] Calcagnotto M, Ponge D, Demir E, et al. Orientation gradients and geometrically necessary dislocations in ultrafine grained dual-phase steels studied by 2D and 3D EBSD. Materials Science and Engineering: A, 2010, 527(10–11): 2738–2746.
[36] Jiang L, Yang H, Yee J K, et al. Toughening of aluminum matrix nanocomposites via spatial arrays of boron carbide spherical nanoparticles. Acta Materialia, 2016, 103: 128–140.
[37] Rozman N, Medved J, Zupanič F. Microstructural evolution in Al-Mn-Cu-(Be) alloys. Philosophical Magazine, 2011, 91(33): 4230–4246.
[38] Zan Y N, Zhou Y T, Li X N, et al. Enhancing high-temperature strength and thermal stability of Al_2O_3/Al composites by high-temperature pre-treatment of ultrafine Al powders. Acta Metallurgica Sinica (English Letters), 2020, 33: 913–921.
[39] Poletti C, Balog M, Simancik F, et al. High-temperature strength of compacted sub-micrometer aluminium powder. Acta Materialia, 2010, 58(10): 3781–3789.
[40] Zan Y N, Zhou Y T, Liu Z Y, et al. Microstructure and mechanical properties of (B_4C+Al_2O_3)/Al composites designed for neutron absorbing materials with both structural and functional usages. Materials Science and Engineering: A, 2020, 773: 138840.
[41] Zhang H, Liu F, Ungar G, et al. A regime beyond the Hall-Petch and inverse-Hall-Petch regimes in ultrafine-grained solids. Communications Physics, 2022, 5: 329.
[42] Chawla N, Shen Y L. Mechanical behavior of particle reinforced metal matrix composites. Advanced Engineering Materials, 2001, 3(6): 357–370.
[43] Nardone V C, Prewo K M. On the strength of discontinuous silicon carbide reinforced aluminum composites. Scripta Metallurgica, 1986, 20(1): 43–48.
[44] Tabandeh-Khorshid M, Ferguson J B, Schultz B F, et al. Strengthening mechanisms of graphene- and Al_2O_3-reinforced aluminum nanocomposites synthesized by room temperature milling. Materials & Design, 2016, 92: 79–87.
[45] Zan Y N, Zhou Y T, Zhao H, et al. Enhancing high-temperature strength of (B_4C+Al_2O_3)/Al designed for neutron absorbing materials by constructing lamellar structure. Composites, Part B: Engineering, 2020, 183: 107674.
[46] Balog M, Krizik P, Nosko M, et al. Forged HITEMAL: Al-based MMCs strengthened with nanometric thick Al_2O_3 skeleton. Materials Science and Engineering: A, 2014, 613: 82–90.